A Cross-Polarization Suppressed Probe-Fed Patch Antenna and Its Applications to Wide-Angle Beam-Scanning Arrays

Hao Chen and Ke-Li Wu, *Fellow, IEEE*

***Abstract*— In this article, H-plane cross-polarization (X-pol) radiation of probe-fed air-filled patch antennas is substantially suppressed by introducing two or more floating metal cylinders underneath the patch, respectively. The X-pol is canceled by the radiation of induced currents on metal cylinders. The working principle of the new X-pol suppressed patch (XSP) antenna is revealed by an approximate model. The X-pol level of a typical XSP antenna can be suppressed to lower than −49 and −37 dB theoretically and experimentally for $|\theta| \leq 60°$. Two 1 × 8-element arrays constructed by XSP antennas and conventional patch antennas are prototyped and measured at scanning beam angles of $\theta = 0°$, −40°, and −65°. The measured co-polarization (co-pol) gain of the XSP antenna array is 0.7 and 0.9 dB larger than that of the conventional patch array at $\theta = -40°$ and −65°, respectively. Besides, the beam scanning angle with −30 dB X-pol level of the XSP antenna array can be as wide as $|\theta| \leq 40°$, while that of the conventional patch array is about $|\theta| \leq 12°$. A wide-band dual-polarized XSP antenna is also presented. The measured maximum H-plane X-pol level can be lower than −29 dB within 8.7% fractional bandwidth.**

***Index Terms*— Antenna array, beam scanning, cross-polarization (X-pol), dual-polarization antenna, patch antenna.**

I. Introduction

IN THE past four decades, the patch antenna is considered as one of the most popular radiation elements in various applications due to its attractive features such as low profile, lightweight, low cost, easy fabrication, and more. Many research efforts have been devoted to the explorations of potentials of the probe-fed patch antennas for broadening the impedance matching bandwidth [1]–[3] and suppressing the cross polarization (X-pol) radiation [6]–[24], among which the stacked patch antenna [1] and the patch antenna with a "U"-shaped slot [2] can create an extra resonant mode, and an "L"-shaped capacitive feeding probe can partially cancel the inductance of the probe and broaden the matching bandwidth [3].

In practice, many patch antennas require an ultra-low X-pol level for wide-angle scanning arrays. For example, polarization purity is an important parameter in the phased array for meteorological measurements, which is a major determinant of the measurement accuracy [4], [5]. Despite the attractive features of a probe-fed air-filled patch antenna, its high H-plane X-pol level needs to be suppressed in many array applications in which a wide-angle scanning is required.

There is a rich literature concerning the reduction of the X-pol level of probe-fed patch antenna in the H-plane. One straightforward method is to change the ground structure, such as reshaping the ground plane to a "U" shape [6] or a "W" shape [7] to reduce the X-pol level to about −20 dB. It is also found that the X-pol level can be reduced by adding shorting pins or shorting wall to the patch radiator but with the payoff of enlarged patch size and the limitation for dual-polarized antenna applications [8]–[12]. In [13], two long folded open-ended stubs are introduced at two corners of the patch radiator to suppress the X-pol level of a shorted patch antenna in the H-plane. A folded air-filled patch structure along the E-plane is used for suppressing the X-pol in the H-plane to a certain low level [14]. But the structure lacks the flexibility of tuning to optimal X-pol suppression.

The differential feed structure is effective for suppressing the X-pol level of a probe-fed patch antenna [15]–[18]. However, the required balun circuit makes the feeding network for a dual-polarized patch antenna complicated. A self-cancellation of the X-pol by the feeding probe requires a half wavelength long structure if the space is permitted as a current null is required to cancel out of the radiation from the two opposite current components [19]. By adopting this concept, an excessively long probe is folded into a meandered line and is squeezed underneath the radiation patch [20]–[22]. An engineered feeding structure with controlled reactance is used to suppress the X-pol radiation in [23]. Although changing the feeding structure can suppress the X-pol radiation to a certain low level, it requires sufficient height of the patch to accommodate the intricate structure.

The above-mentioned methods, either reshaping the patch or the ground plane, or modifying the feeding structure of the patch antenna, can only suppress the X-pol of a probe-fed patch antenna to a certain level. Additionally, these methods cannot independently control the X-pol level without sacrificing other antenna attributes or occupying more spaces. Antennas with an independently controllable X-pol level are useful in array antenna applications, in which the X-pol level may be easily affected by the unsymmetrical surrounding near

Manuscript received 16 April 2021; revised 4 November 2021; accepted 7 December 2021. Date of publication 11 January 2022; date of current version 6 October 2022. This work was supported in part by the Research Grants Council of the Hong Kong Special Administrative Region, China, under Grant 14205217. *(Corresponding author: Ke-Li Wu.)*

The authors are with the Department of Electronic Engineering, The Chinese University of Hong Kong, Hong Kong (e-mail: haochen393@link.cuhk.edu.hk; klwu@cuhk.edu.hk).

Color versions of one or more figures in this article are available at https://doi.org/10.1109/TAP.2022.3140328.

Digital Object Identifier 10.1109/TAP.2022.3140328

0018-926X © 2022 IEEE. Personal use is permitted, but republication/redistribution requires IEEE permission.
See https://www.ieee.org/publications/rights/index.html for more information.

Authorized licensed use limited to: Chinese University of Hong Kong. Downloaded on July 27,2023 at 06:40:54 UTC from IEEE Xplore. Restrictions apply.

the antenna or the mutual coupling between antenna elements. Ground Defected Structure (DGS) is an effective scheme to independently reduce the X-pol level by etching slots on the ground plane under or near the patch antenna [24]. However, since the length of slots is comparable to the wavelength to provide sufficient X-pol suppression, DGS may inevitably increase unwanted backward radiation.

In this article, a new air-filled patch antenna structure that can realize an extremely low X-pol level is proposed for the first time. The antenna structure consists of several electrically small floating metal cylinders underneath the patch radiator. The currents induced on the metal cylinders create controllable interfering radiation fields to cancel out the X-pol radiation caused by the feeding probe. Compared to the existing X-pol cancellation methods, the new antenna configuration possesses the following unique interesting features.

1) No additional space is required and the patch size is comparable to the conventional air-filled patch antennas.
2) No extra backward radiation is introduced.
3) The X-pol level in the H-plane can be deeply suppressed virtually in a wide-angle range.
4) More importantly, it can be applied to a dual-polarized probe-fed patch antenna, which enables the probe-fed patch antenna to be a promising candidate for the wireless applications where dual-polarized patch antennas are needed.

This article is organized as follows. In Section II-A, the working principle of the proposed antenna configuration will be discussed in detail. EM simulated and measured results of a linearly polarized X-pol suppressed patch (XSP) antenna are presented to demonstrate its main features in Section II-B. Section II-B also shows some parametric studies for better understanding the design guideline. In Section II-C, two 1×8 linearly polarized antenna arrays constructed by the proposed XSP antenna and conventional probe-fed air-filled patch antenna are prototyped and measured at different beam scanning angles. A wideband dual-polarized patch antenna with suppressed X-pol level is also presented, which is supported with the simulated and measured results in Section III. A comparison between the proposed XSP antennas and some of the existing probe-fed patch antennas with suppressed X-pol level is made to show the superiority of the new antenna configuration, followed by conclusion.

II. Antenna Structure and Working Principle

After introducing the antenna configuration, the working principle of the proposed XSP antenna will be presented in this section. Some major parameters of the XSP antenna will be studied for providing a design guideline. In addition, two 1×8 antenna arrays formed by the XSP antennas and the conventional air-filled patch antennas are measured and compared at three different beam scanning angles to demonstrate the superiority of the XSP antenna in wide-angle beam-scanning arrays.

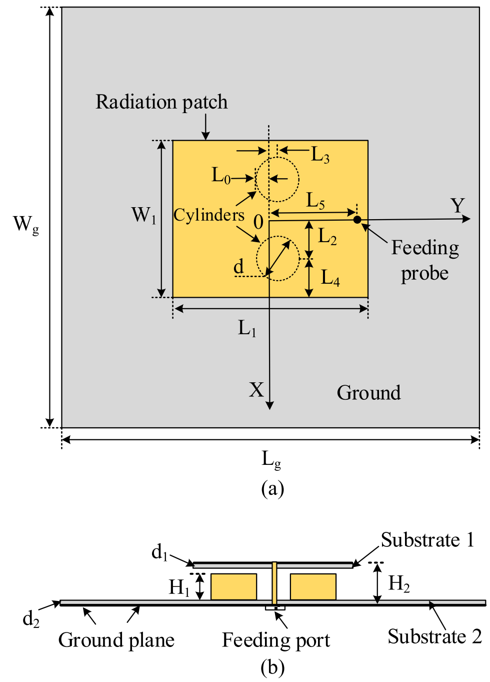

Fig. 1. Geometry and dimensions of the proposed linearly polarized XSP antenna. (a) Front view. (b) Side view.

A. XSP Antenna Structure and Working Principle

The geometry of an exemplary linearly polarized XSP antenna is shown in Fig. 1. The XSP antenna consists of a radiating patch, a feeding probe, the ground plane, and two floating metal cylinders that are perpendicularly placed between the patch and the ground plane without contact. Other number of cylinders may also serve the purpose. In the demonstration example, the patch radiator is printed on a thin Panasonic R5725 substrate (substrate 1) with $\varepsilon_r = 4.1, \tan\delta = 0.006$, and thickness ($d_1$) of 0.8 mm. The two floating metal cylinders situate on a grounded substrate of an FR4 substrate (substrate 2) with $\varepsilon_r = 4.3, \tan\delta = 0.02$, and thickness ($d_2$) of 0.8 mm. The substrate keeps the cylinders from being grounded. A simple gasket between the cylinders and the ground can also serve the purpose. The two floating cylinders are placed symmetrically along the YoZ-plane and are offset toward the feeding probe, which is located on the $+Y$-axis. The height of the patch from the ground plane is not critical. Since there is no noticeable change in the patch size after introducing the metal cylinders, the design rule for probe fed air-filled patch antennas is still applicable.

An effective way to show the working principle is through investigating the current distribution on the XSP antenna. Setting the origin of the coordinate system on the ground plane at the center of the patch. With reference to Fig. 1, for a patch antenna polarized in the Y-direction and resonating at frequency of 2.45 GHz with the TM_{01} mode, the patch sizes are $L_1 = 54$ mm (0.44λ), $W_1 = 43$ mm (0.35λ), and height $H_2 = 8$ mm (0.065λ), where λ is the wavelength at 2.45 GHz. The feeding probe is located on the Y-axis and is away from the patch center by $L_5 = 23.5$ mm. The diameter of the feeding

Authorized licensed use limited to: Chinese University of Hong Kong. Downloaded on July 27,2023 at 06:40:54 UTC from IEEE Xplore. Restrictions apply.

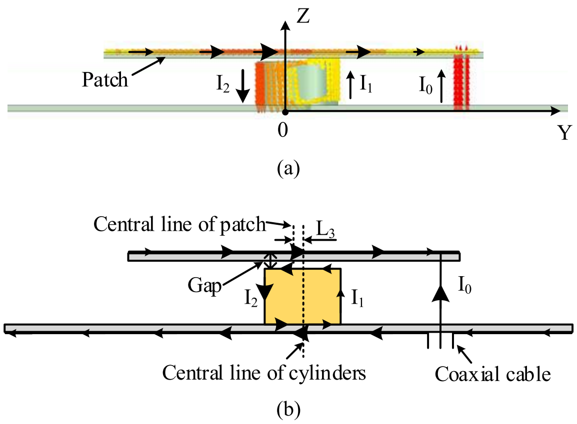

Fig. 2. (a) EM simulated current distribution on an XSP antenna. (b) Simplified current distribution on the XSP antenna.

probe is 1.3 mm. The two cylinders are with a diameter d of 11.2 mm, height $H_1 = 5.9$ mm, and are offset from the center in two opposite X-directions by $L_2 = 9.5$ mm and in positive Y-direction by $L_3 = 1.2$ mm.

Fig. 2(a) shows the EM simulated current distribution by HFSS on the cylinders and the feeding probe of the linearly polarized XSP antenna at the resonance frequency. Only the current distribution on a non-radiating edge is shown for simplicity. In generating the current distribution, the time instance in a cycle that best presents the essence of the current is chosen. It can be observed that the current on the feeding probe can be assumed to be uniformly distributed with constant current I_0. Although additional X-pol radiation and a slight distortion on the E-plane co-polarization (co-pol) gain pattern may occur due to higher order modes for some patch antenna structures, in which the length of the radiating edge is close to a multiple of that of the non-radiating edge [12], this phenomenon is not a concern in this study. It will be demonstrated that the proposed linearly polarized XSP antenna can cancel the parasitic radiation from the feeding probe by using the metal cylinders, leading to an extremely low X-pol level in the H-plane.

The current induced on the surfaces of the two metal cylinders underneath the patch concentrates on two sides: the side facing to the feeding probe and the side facing toward to opposite direction. The current on the two sides is in opposite directions, and therefore, forming a current loop. By ignoring the induced currents on the top and bottom surfaces of the cylinders which have no effects on the X-pol radiation, as illustrated in Fig. 2(b), the induced currents on the two mentioned side surfaces can be considered as two lumped currents, I_1 and I_2, respectively. Since the two cylinders are offset from the central line leaning to the feeding probe by L_3 distance, the side surface that is closer to the current maximum on the radiation patch the current, I_2 is larger in magnitude than that of I_1. Interestingly, current I_2 is in the opposite direction as that of I_0 on the feeding probe, and the X-pol radiation caused by the feeding probe can be effectively canceled.

To justify the cancellation principle, a simplified model of the vertically oriented currents of an XSP antenna with their

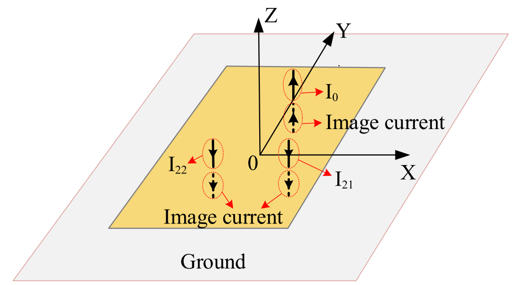

Fig. 3. Simplified feeding probe current I_0, cylinder currents I_{21} and I_{22} of an XSP antenna, and their image currents.

image currents is shown in Fig. 3, in which current I_1 is omitted for simplicity due to its negligible amplitude, I_0 is the current on the feeding probe, and I_{21} and I_{22} represent the induced currents on the two side-by-side cylinders, respectively. Current I_0 is centered at $(0, L_5, H_2/2)$ and its image current is centered at $(0, L_5, -H_2/2)$, forming a dipole array along the Z-direction. H_2 is the height of the feeding probe of the patch antenna. L_5 is the offset distance of the feeding probe from the patch center along the Y-axis. The electric far-field of the array with a constant current magnitude I_0 can be easily found as

$$\mathbf{E}_{I_0} = \mathbf{a}_\theta j \frac{\eta_0 I_0 e^{-jkr}}{2\pi r} e^{jkL_5 \sin(\theta)\sin(\phi)} \sin(kH_2\cos(\theta))\tan(\theta) \quad (1)$$

where η_0 and k are the wave impedance and wavenumber, respectively, in free space.

Since the two cylinders are symmetrically placed along the Y-axis, currents I_{21} and I_{22} are with the same magnitude of I_2 and are oriented in the opposite direction to that of I_0. The center coordinators for the two cylinder currents are $(L_2, -L_0, H_1/2 + d_2)$ and $(-L_2, -L_0, H_1/2 + d_2)$, where L_0 and L_2 are the offset distances of the filament current I_2 from the center line of the patch antenna in the Y- and X-directions, respectively. By the same token, the electric far-field radiated by the induced currents I_{21} and I_{22}, and their image currents, can be found as, respectively,

$$\begin{aligned}\mathbf{E}_{I_{21}} &= -\mathbf{a}_\theta j \frac{\eta_0 I_2 e^{-jkr}}{\pi r} e^{jk(L_2\sin(\theta)\cos(\phi) - L_0\sin(\theta)\sin(\phi))} \\ &\quad \cdot \sin\left(\frac{kH_1\cos(\theta)}{2}\right)\cos\left(k\left(\frac{H_1}{2}+d_2\right)\cos(\theta)\right)\tan(\theta)\end{aligned} \quad (2a)$$

$$\begin{aligned}\mathbf{E}_{I_{22}} &= -\mathbf{a}_\theta j \frac{\eta_0 I_2 e^{-jkr}}{\pi r} e^{jk(-L_2\sin(\theta)\cos(\phi) - L_0\sin(\theta)\sin(\phi))} \\ &\quad \cdot \sin\left(\frac{kH_1\cos(\theta)}{2}\right)\cos\left(k\left(\frac{H_1}{2}+d_2\right)\cos(\theta)\right)\tan(\theta).\end{aligned} \quad (2b)$$

The total electric far filed in the H-plane ($\phi = 0$) contributed by the currents on the feeding probe and the two cylinders is the sum of the fields in (1), (2a), and (2b), which can be expressed as (3), as shown at the bottom of the next page.

As can be seen from (3) that the vertical currents contribute only the θ-component of the electric field, which is the X-pol radiation in the H-plane. If the height of the XSP antenna H_2 and the spacing of the cylinders to the ground plane, d_2, are

Authorized licensed use limited to: Chinese University of Hong Kong. Downloaded on July 27,2023 at 06:40:54 UTC from IEEE Xplore. Restrictions apply.

TABLE I
VALUE OF PARAMETERS OF THE XSP PATCH ANTENNA UNIT (mm)

W_g	L_g	L_1	L_2	L_3	L_4	L_5
150	150	54	9.5	1.2	12	23.5
L_0	W_1	H_1	H_2	d	d_1	d_2
4.4	43	5.9	8	11.2	0.8	0.8

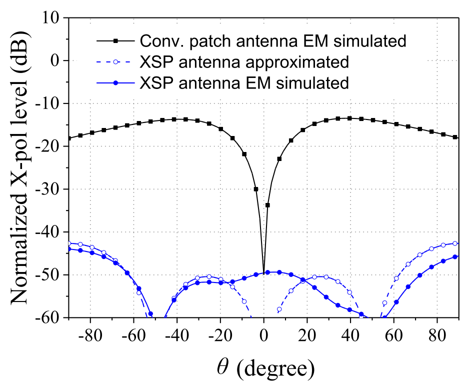

Fig. 4. EM simulated and approximately modeled X-pol level (normalized to the peak co-pol gain) of an XSP antenna and the EM simulated X-pol level of a conventional air-filled patch antenna.

fixed, by carefully choosing H_1, L_2, and L_3 for tactically creating I_2, the electric field radiated by the vertical currents in the H-plane can be totally canceled at a specific θ-direction. In other words, the magnitude of I_2 is determined by the "gap" between the cylinders and the patch, the offset distance L_3, and the diameter of the cylinders d. It is worth mentioning that the vertical currents I_{21} and I_{22} also affect the E-plane co-pol gain pattern in the level of -15 dB when compared to the peak co-pol gain as the cancellation takes place in the level.

B. Linearly Polarized XSP Antenna

To demonstrate the working principle, a linearly polarized XSP antenna working at 2.45 GHz is parametrically studied using HFSS. The TM_{01} mode is excited in the patch antenna so that the length of the patch antenna L_1 is about half a wavelength. The height of the antenna is not critical and is chosen to be 8 mm. The positions and sizes of the two cylinders are finetuned by EM simulation to realize good X-pol cancellation. While other parameters of the patch are finetuned to achieve good matching condition at 2.45 GHz. The detailed sizes of the linearly polarized XSP antenna are listed in Table I. For comparison purpose, a conventional probe-fed air-filled patch antenna with sizes of 51 mm $\times$ 43 mm $\times$ 8 mm is also designed. The conventional patch also excites the TM_{01} mode and has the same height and width as those of the XSP antenna.

Fig. 4 shows the comparison of the H-plane X-pol level of the XSP antenna and the conventional air-filled patch

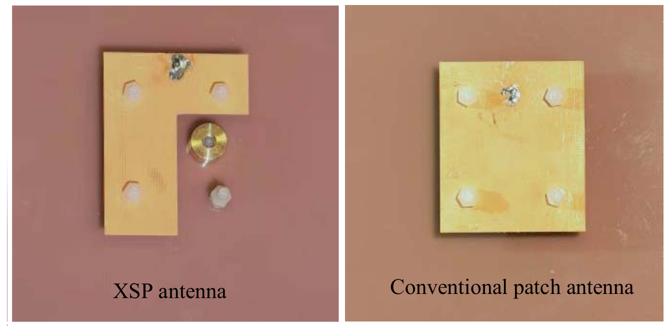

(a) (b)

Fig. 5. (a) Photograph of the prototyped linearly polarized XSP antenna (with patch partially cut-off). (b) Photograph of the reference conventional probe-fed air-filled patch antenna.

antenna. The X-pol gain of the conventional patch antenna and the XSP antenna are normalized to their peak co-pol gain. In the figure, the EM-simulated X-pol levels of the two patch antennas are shown in the solid dotted lines and the approximately estimated X-pol levels of the XSP antenna according to (3) are superposed using dashed-dotted lines. It can be observed that the results of the HFSS EM model and the approximated model agree well in a wide-angle range. The simulated maximum X-pol level in the H-plane of the conventional air-filled patch antenna is about -15 dB at about $\theta = \pm 40°$, whereas that of the XSP antenna can be lower than -49 and -44 dB within the angle range of $|\theta| \leq 60°$ and $|\theta| \leq 90°$, respectively. To achieve a wide X-pol suppression angle range, the totally X-pol cancellation angle is tuned at $\theta = \pm 50°$. The linearly polarized XSP antenna as well as the linearly polarized conventional air-filled patch antenna are prototyped and measured. The electric size of the prototyped XSP antenna and the conventional air-filled patch antenna are $0.44\lambda \times 0.35\lambda \times 0.065\lambda$ and $0.42\lambda \times 0.35\lambda \times 0.065\lambda$, respectively, showing nearly the same electric dimensions. The photographs of the prototyped linearly polarized XSP antenna and the reference conventional patch antenna are shown in Fig. 5. The radiation properties are measured using the SATIMO SG-128 spherical scanner system in the Radio-Frequency Radiation Research Laboratory of the university. In the gain measurement, the system is calibrated with the standard horn antenna.

The EM simulated (dashed-dotted line) and the measured (solid dotted line) reflection coefficients of the prototyped XSP antenna and those of the conventional air-filled patch antenna are shown in Fig. 6. The -10 dB reflection coefficient fractional bandwidth of the XSP antenna and the conventional patch antenna are about 6.1% and 7.7%, respectively. Fig. 7 shows the EM simulated and measured radiation patterns (normalized to the peak co-pol gain) of the XSP antenna and the conventional patch antenna. The measured maximum co-pol gain at 2.45 GHz of the XSP antenna is 9.6 dBi,

$$\mathbf{E} = \mathbf{a}_\theta j \frac{\eta e^{-jbr}}{2\pi r} \tan(\theta)\sin(kH_2\cos(\theta)) \cdot \left(I_0 - 4I_2 \frac{\sin\left(k\frac{H_1}{2}\cos(\theta)\right)\cos\left(k\left(\frac{H_1}{2}+d_2\right)\cos(\theta)\right)\cos(kL_2\sin(\theta))}{\sin(kH_2\cos(\theta))} \right) \quad (3)$$

Authorized licensed use limited to: Chinese University of Hong Kong. Downloaded on July 27,2023 at 06:40:54 UTC from IEEE Xplore. Restrictions apply.

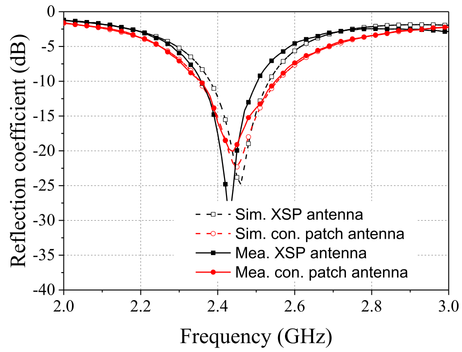

Fig. 6. EM simulated and measured reflection coefficients of the prototyped XSP antenna and the conventional air-filled patch antenna.

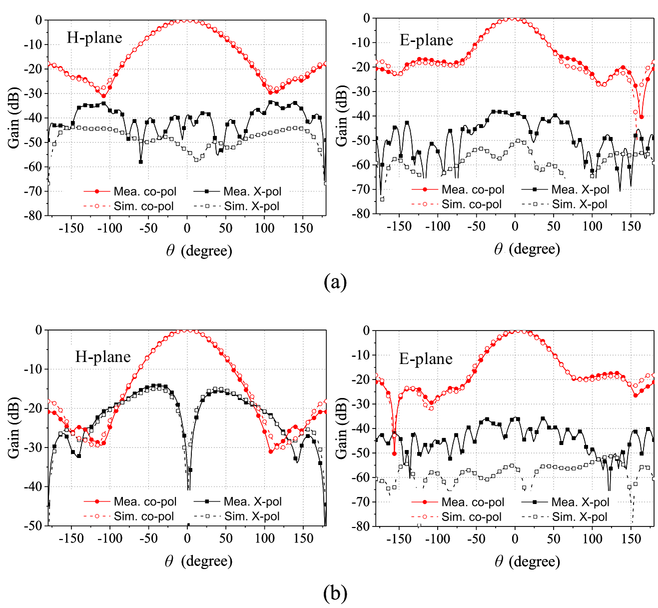

Fig. 7. EM simulated and measured radiation patterns of (a) prototyped XSP antenna and (b) conventional patch antenna.

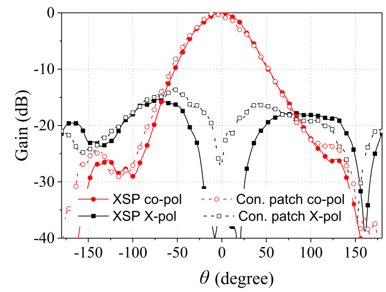

Fig. 8. Measured radiation patterns (normalized to the peak co-pol gain) of the XSP antenna and the conventional patch antenna in diagonal plane $\phi = 45°$.

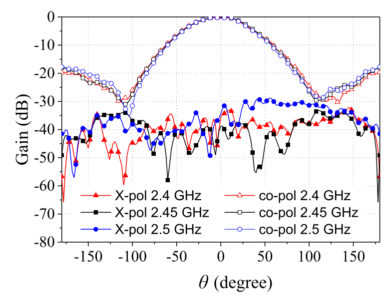

Fig. 9. Measured H-plane radiation patterns (normalized to the peak co-pol gain) of the XSP antenna at 2.4, 2.45, and 2.5 GHz.

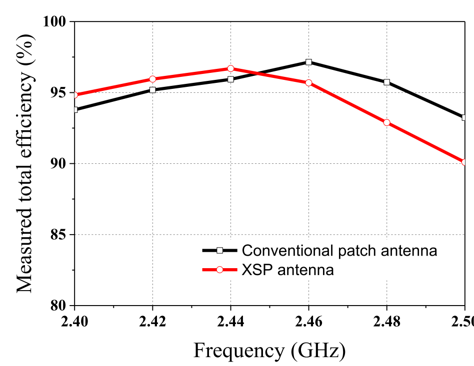

Fig. 10. Measured total efficiencies of the prototyped XSP antenna and the conventional patch antenna.

whereas that of the conventional patch antenna is 9.7 dBi. The measured maximum H-plane X-pol level of the XSP antenna and the conventional patch antenna are about -37 and -15 dB, respectively, within the angle range of $|\theta| \leq 60°$. The difference between the measured and simulated H-plane X-pol level of the XSP antenna is mainly due to fabrication error in controlling the "gap" between the cylinders and the patch and the symmetry of the two cylinders. The comparison of the measured radiation patterns normalized to the peak gain in the $\phi = 45°$ plane between the XSP antenna and the conventional patch antenna is shown in Fig. 8. The co-pol and X-pol gain in the diagonal plane can be calculated according to [25]. The X-pol of the XSP antenna in the diagonal plane is still obviously lower than that of the conventional patch antenna within $|\theta| \leq 60°$. The measured H-plane radiation patterns of the XSP antenna at the center frequency and two band edge frequencies, that is, 2.45, 2.4, and 2.5 GHz, are superimposed in Fig. 9, showing stable X-pol suppression across the whole frequency band. The measured total efficiencies of the XSP antenna and the conventional air-filled patch antenna are plotted in Fig. 10, showing more than 90% efficiencies from 2.4 to 2.5 GHz for both cases. The peak efficiencies of the XSP antenna and the air-filled patch antenna across the band are about 96% and 97%, respectively. But the overall efficiencies of the XSP antenna is a bit worse than that of the conventional patch due to the narrower bandwidth of the XSP antenna when compared to the conventional patch antenna.

To better understand the H-plane X-pol cancellation principle, the critical design parameters are studied. When offset >0, as illustrated in Fig. 11(a), the vertical current I_2 on each cylinder is in the opposite direction as that of I_0 on the feeding probe. This will result in X-pol cancellation. However, when offset <0, as illustrated in Fig. 11(b), current I_1 on each cylinder becomes dominant and is oriented in the same direction as that of I_0, resulting in increased X-pol radiation.

Authorized licensed use limited to: Chinese University of Hong Kong. Downloaded on July 27,2023 at 06:40:54 UTC from IEEE Xplore. Restrictions apply.

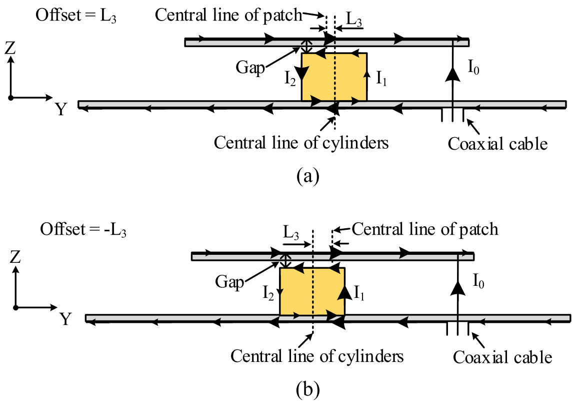

Fig. 11. Current distribution on the XSP antenna with different offset direction of cylinders along the Y-axis. (a) Offset $L_3 > 0$. (b) Offset $L_3 < 0$.

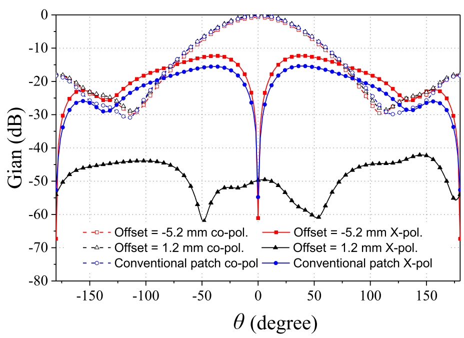

Fig. 12. H-plane radiation patterns (normalized to the peak co-pol gain) of the conventional patch antenna and the XSP antenna with different offset L_3.

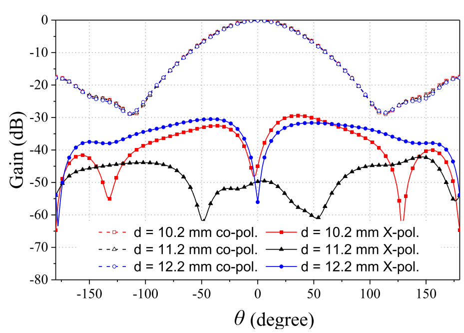

Fig. 13. H-plane radiation patterns of the XSP antenna with different diameter d of cylinders.

Fig. 12 presents how the H-plane X-pol level, which is normalized to the peak co-pol gain, changes with different offset. It is interesting to find that when the offset $L_3 = 1.2$ mm, the X-pol level can be reduced to lower than -49 dB for $|\theta| \leq 60°$. Oppositely, when the offset $L_3 = -5.2$ mm, the maximum X-pol level is increased to about -12 dB, which is 3 dB higher than that of the conventional air-filled patch antenna.

The magnitude of the dominant vertical current on two cylinders is determined by the coupling strength between the cylinders and the patch, which means that the diameter of the cylinders and the "gap" between the patch and the cylinders are the controlling factors. Fig. 13 shows the H-plane radiation pattern of the XSP antenna with different diameters d. It is clearly seen that $d = 11.2$ mm is an optimal choice when compared to the cases of $d = 10.2$ mm and $d = 12.2$ mm. Fig. 14 shows the H-plane radiation pattern of the XSP antenna with different values of the "gap" between the patch and the cylinders.

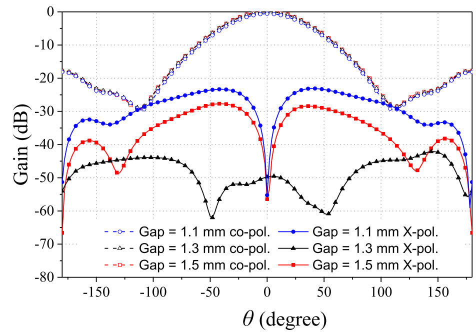

Fig. 14. H-plane radiation patterns of the XSP antenna with different "gap" between cylinders and the radiation patch.

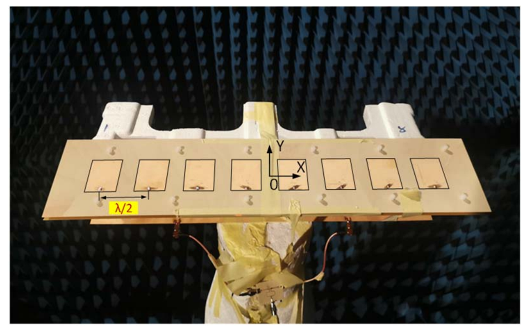

Fig. 15. Photograph of the 1 × 8 linearly polarized XSP antenna array.

C. Application to Wide-Angle Beam-Scanning Arrays

The XSP antenna can find its vital applications in wide-angle beam-scanning arrays. To demonstrate this feature, two 1 × 8 linearly polarized patch antenna arrays constructed by the XSP antenna and conventional probe-fed air-filled patch antenna are fabricated and compared experimentally, showing the necessity of suppressing the H-plane X-pol level for a phased array with a wide beam scanning angle. The fabricated XSP antenna array is shown in Fig. 15. The center-to-center spacing between two adjacent antenna elements is set to 0.5λ at the center frequency of 2.45 GHz. By finetuning the parameters of two cylinders of each XSP antenna element in the array environment, a deep cancellation on H-plane X-pol level can be obtained. To measure the radiation pattern that emulates beam scanning, the Wilkinson power divider with equal power division but progressive phase delay for antenna elements is applied. The progressive phase delay between antenna ports is realized by using connecting coaxial cables of different electric length between antenna ports and a Wilkinson power divider network.

Fig. 16 shows the EM simulated and the measured radiation patterns of the two 1 × 8 arrays at three beam scanning angles ($\theta = 0°$, $-40°$, and $-65°$) at 2.45 GHz. The maximum

Authorized licensed use limited to: Chinese University of Hong Kong. Downloaded on July 27,2023 at 06:40:54 UTC from IEEE Xplore. Restrictions apply.

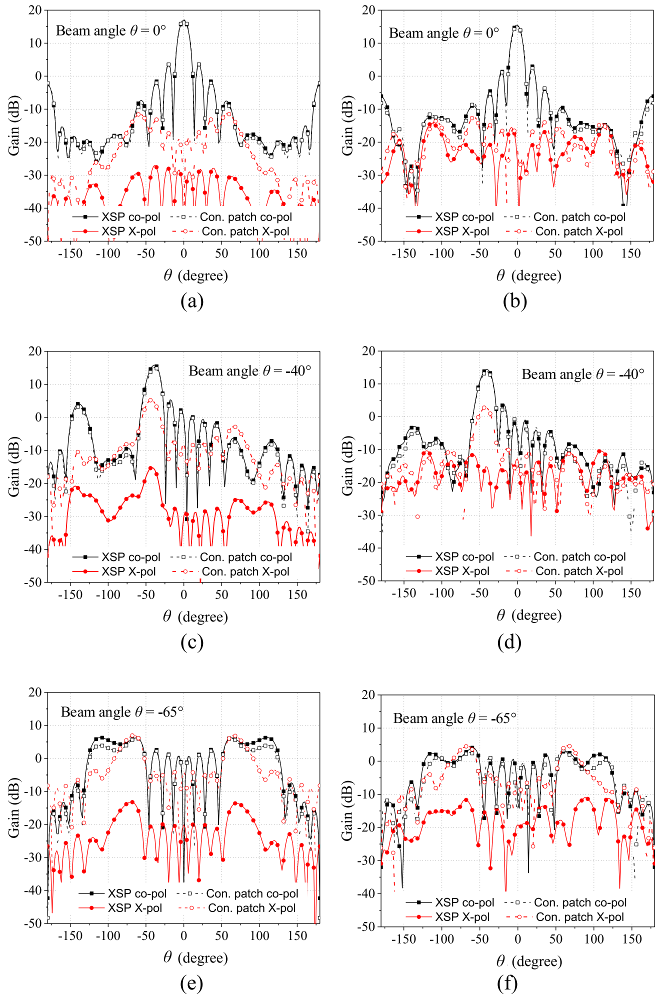

Fig. 16. H-plane radiation patterns of the XSP and conventional patch antenna arrays at different beam scanning angles θ. (a) Simulated at $\theta = 0°$. (b) Measured at $\theta = 0°$. (c) Simulated at $\theta = -40°$. (d) Measured at $\theta = -40°$. (e) Simulated at $\theta = -65°$. (f) Measured at $\theta = -65°$.

co-pol gains, X-pol gains, as well as the total efficiencies at the three beam scanning angles are summarized in Table II. The measured co-pol gains of the XSP antenna array are about 0.7 and 0.9 dB higher than that of the conventional patch antenna array when the beam scanning angle $\theta = -40°$ and $-65°$, respectively. The gain enhancement is contributed by the significant reduction of the unwanted X-pol radiation. Since the maximum co-pol gains of the XSP antenna array and the conventional patch antenna array in the boresight direction $\theta = 0°$ are 15.4 and 15.3 dB, respectively, the scan loss of the XSP antenna is about 0.6 and 0.8 dB lower than that of the conventional patch antenna array for $\theta = -40°$ and $\theta = -65°$, respectively. The measured X-pol levels of the XSP antenna array at the three scanning angles are significantly smaller than those of the conventional air-filled patch antenna array. The beam scanning angle range with lower than -30 dB X-pol level (normalized to the peak co-pol gain) of the XSP antenna array is about $|\theta| \leq 40°$, while that of the conventional air-filled patch array is only about $|\theta| \leq 12°$. In particular, at $\theta = 0°$ and $-40°$, the measured X-pol level of the XSP antenna array is as low as -41.4 and -30.9 dB, respectively.

TABLE II

Simulated and Measured Peak Co-Pol and X-Pol Gains (in dBi) and Measured Total Efficiencies at Three Scanning Angles

		θ = 0°		θ = -40°		θ = -65°	
		Co-pol	**X-pol**	**Co-pol**	**X-pol**	**Co-pol**	**X-pol**
Sim.	XSP array	16.9	-35	15.4	-14.9	6.1	-13.4
	Conv. array	16.9	-38	14.8	4.8	5.7	7
Mea.	XSP array	15.4	-26	14.4	-16.5	3.5	-12.6
	Total efficiency of XSP array	69%		63%		50%	
	Conv. array	15.3	-22	13.7	2.6	2.6	4.5
	Total efficiency of Conv. array	70%		64%		60%	

Most significantly, at $\theta = -65°$, which is the extreme beam scanning angle of the arrays with 180° progressive phase shift, the measured X-pol level of the XSP antenna array is -12.6 dB, whereas that of the conventional air-filled patch array is $+4.5$ dB. It is worthy to mention that the mutual coupling between two adjacent antenna elements in the XSP antenna array and the conventional patch antenna array are at the level of -14 and -17 dB, respectively. The measured total efficiencies of the two antenna arrays are comparable when $\theta = 0°$ and $-40°$. However, when $\theta = -65°$, the measured total efficiency of the XSP antenna array is about 10% lower than that of the conventional patch antenna array due to the higher mutual coupling of the XSP array that causes poorer active matching condition. The EM simulation shows that the worst active reflection coefficient of the XSP array for scanning angle of $\theta = -65°$, which is occurred at the ports of the center elements, is about -5 dB and the best active reflection coefficient is about -11 dB. Since the reflected power due poor active reflection coefficient is absorbed by the Wilkinson power divider network, about 20% efficiency degradation at $\theta = -65°$ is observed. Although the total efficiency for the array with conventional patch is higher at $\theta = -65°$, the peak co-pol gain for the XSP array is still 0.8 dB higher than that of the array with conventional patch attributed by the suppression of X-pol radiation. One can reduce the mutual coupling by various means, such as the array-antenna decoupling surface (ADS) technique [26]. The loss of the feeding network also contributes to the drop of the measured gain significantly in both XSP and conventional air-filled patch antenna arrays when compared to those of the EM simulated results given in Table II.

III. Dual-Polarized XSP Antenna With Enhanced Matching Bandwidth

The XSP configuration can be extended to a dual-polarized stacked XSP antenna with enhanced matching bandwidth. Again, for comparison purpose, a dual-polarized stacked normal patch (NP) antenna is also fabricated and measured. The geometry of the dual-polarized XSP antenna is depicted in Fig. 17(a) and (b). The photographs of the prototyped dual-polarized NP antenna and XSP antenna are shown in Fig. 17(c) and (d), respectively. The stacked dual-polarized

Authorized licensed use limited to: Chinese University of Hong Kong. Downloaded on July 27,2023 at 06:40:54 UTC from IEEE Xplore. Restrictions apply.

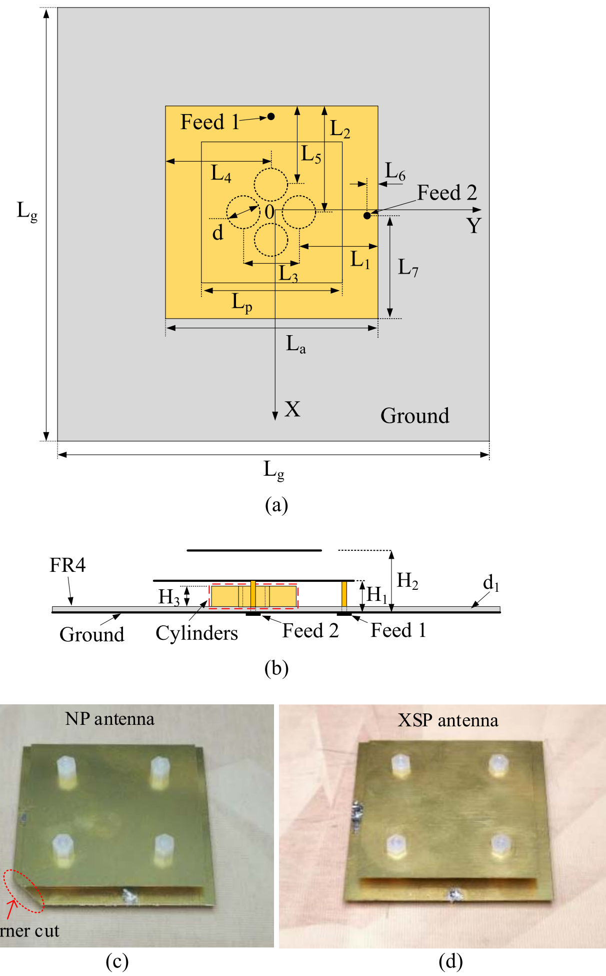

Fig. 17. (a) Top view and (b) side view of a dual-polarized XSP antenna. (c) Photograph of the prototyped NP antenna. (d) Photograph of the prototyped XSP antenna.

TABLE III

DIMENSIONS OF PROTOTYPED DUAL-POLARIZED STACKED XSP ANTENNA UNIT (mm)

L_g	L_a	L_p	L_1	L_2	L_3	L_4	L_5
150	61	53.2	22	30.5	17	30.5	22
L_6	L_7	H_1	H_2	H_3	d	d_1	
2.5	29.5	4	9	2.9	11	0.8	

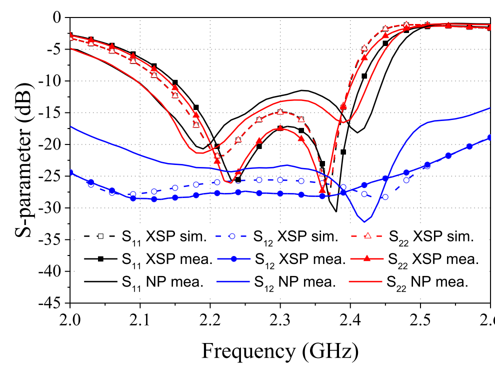

Fig. 18. Simulated and measured S-parameters of the prototyped XSP antenna and the measured S-parameters of the reference NP antenna.

XSP antenna consists of two radiating patches, two independent feeding probes, one for each polarization, the ground plane, and four floating metal cylinders. The antenna size is about $0.47\lambda \times 0.47\lambda \times 0.07\lambda$, while the ground size is about $1.15\lambda \times 1.15\lambda$, all at 2.3 GHz. According to the design rule of a stacked patch antenna, the sizes of the two radiation patches are tuned to generate two resonant notches at 2.22 and 2.38 GHz to realize a wide matching bandwidth. The positions of the four cylinders are located underneath the lower radiation patch. The size and the positions of the four cylinders are finetuned to realize good H-plane X-pol suppression within the frequency band. The two feeding probes are slightly offset from the center lines toward the corner between them to realize good ports isolation. The details of all physical parameters are listed in Table III. To make a reasonable comparison, the total size of the NP antenna is also $0.47\lambda \times 0.47\lambda \times 0.07\lambda$, which is the same as the XSP antenna. However, to achieve acceptable ports isolation and matching condition of the NP antenna, the corner between two ports is cut a bit.

The dual-polarized XSP antenna and the NP antenna are fabricated using the FR4 substrate for ground plane and copper sheets with a thickness of 0.3 mm for the two stacked patches. The EM simulated and measured S-parameters of the prototyped XSP antenna and the measured S-parameters of the NP antenna are superimposed in Fig. 18. The simulated and measured results of the XSP antenna agree well and the performance of the NP antenna is comparable to that of the XSP antenna. The measured -10 dB reflection coefficient bandwidth of the XSP antenna is about 11%, from 2.14 to 2.4 GHz, while the -15 dB reflection coefficient bandwidth is about 9%, from 2.18 to 2.39 GHz. The isolation between the two ports is better than 27 dB within the -10 dB reflection coefficient bandwidth. Fig. 19 illustrates the measured gain patterns, which is normalized to the peak co-pol gain, of the XSP antenna and the NP antenna at 2.22 and 2.38 GHz, showing similar co-pol radiation patterns in both E- and H-planes. However, the X-pol levels of both E- and H-planes of the XSP antenna are obviously lower than those of the NP antenna, showing lower than -32 and -28 dB at 2.2 and 2.38 GHz, respectively, for about $|\theta| \leq 90^\circ$. The maximum gain of each polarization of the XSP antenna is about 9.7 dBi, and the measured 3 dB beam widths in the E- and H-planes are about 52° and 64°, respectively. Fig. 20 plots the projected co-pol and X-pol gains (normalized to the peak gain) of the XSP antenna and the NP antenna in the diagonal plane $\phi = 45^\circ$ when antenna 1 is excited and antenna 2 is terminated by 50 Ω load at 2.2 and 2.38 GHz. The X-pol level of the XSP antenna is obviously much lower than that of the NP antenna in the diagonal plane within the angle range of $|\theta| \leq 60^\circ$. The maximum H-plane X-pol level (normalized to the peak co-pol gain) of the two polarization antennas of the XSP antenna as well as their total efficiency versus frequency are presented in Fig. 21, showing that the simulated X-pol levels of the dual-polarized XSP antennas are lower than -30 dB within the -10 dB reflection coefficient bandwidth (11%), whereas the measured X-pol levels of the dual-polarized XSP antennas

Authorized licensed use limited to: Chinese University of Hong Kong. Downloaded on July 27,2023 at 06:40:54 UTC from IEEE Xplore. Restrictions apply.

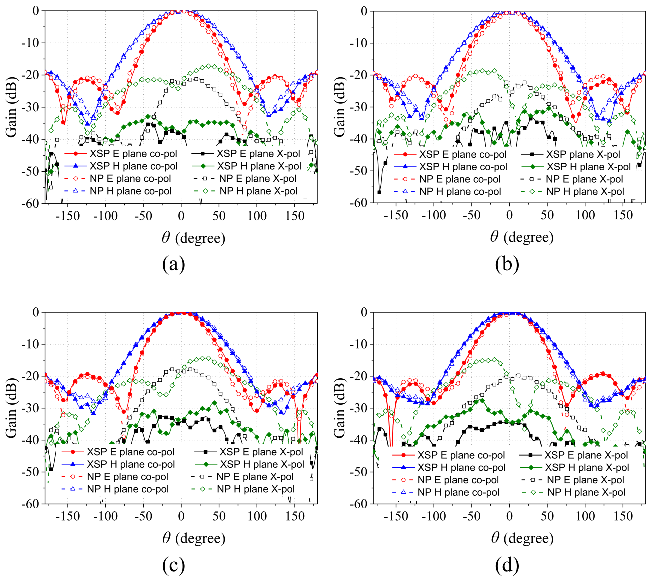

Fig. 19. Measured radiation patterns of the prototyped dual-polarized XSP antenna and the reference NP antenna. (a) Port 1 at 2.22 GHz. (b) Port 2 at 2.22 GHz. (c) Port 1 at 2.38 GHz. (d) Port 2 at 2.38 GHz.

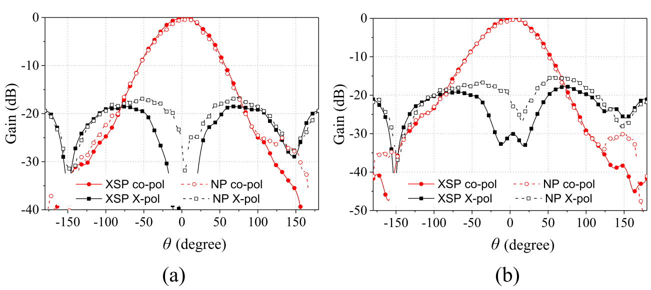

Fig. 20. Measured radiation patterns of the XSP antenna and the NP antenna in diagonal plane $\phi = 45^\circ$ when port 1 is excited and port 2 is terminated by 50 Ω load at (a) 2.2 and (b) 2.38 GHz.

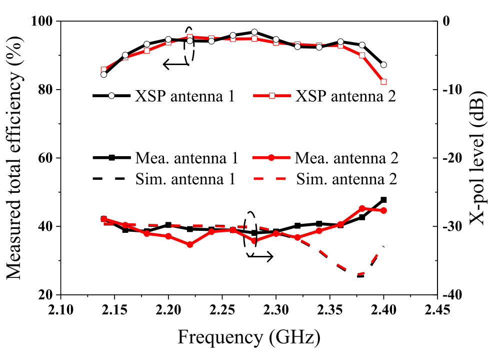

Fig. 21. Simulated and measured maximum H-plane X-pol levels (normalized to the peak co-pol gain) of the dual-polarized XSP antenna and the measured total efficiencies when each of the two antennas is excited and the other antenna is terminated by 50 Ω load.

are lower than −29 and −26 dB within an 8.7% fractional bandwidth from 2.16 to 2.36 GHz and the −10 dB reflection coefficient bandwidth (11%), respectively. The measured total efficiencies of the two polarized antennas of the XSP antenna within the −10 dB reflection coefficient bandwidth are in the range 82%–95%.

TABLE IV

COMPARISON OF EXPERIMENTAL MAXIMUM X-POL IN ANGLE $|\theta| \le 60^\circ$ OF LINEARLY AND DUAL-POLARIZED PATCH ANTENNAS

Ref (year)	**Configuration**	**Polarization / Dual-Polarization**	**Peak Gain (dBi)**	**Max. X-pol (dB)**
[6] 2002	Patch with U-shaped ground	Linear / No	8	-19.6
[11] 2018	Patch with shorting pins	Linear / No	7.4	-34
[15] 1999	Differentially-fed patch	Linear / Yes	7.3	-28
[19] 2003	Patch with suspended probe	Linear / No	5	-20
[24] 2012	Patch with DGS structure	Linear / Yes	6.5	-25
This work	Patch with metal cylinders	Linear / Yes	9.8	-37
[16] 2009	Differentially-fed patch	Dual Polarization	7.4	-23
[22] 2007	Patch with meandered probe	Dual Polarization	10	-18
This work	Patch with metal cylinders	Dual Polarization	9.7	-29

Table IV compares the maximum X-pol level (referring to the peak co-pol gain) within the angle range of $|\theta| \le 60^\circ$ and the peak gain of the XSP antennas and existing probe-fed patch antennas with suppressed X-pol. For linear polarization applications, the XSP patch antenna can achieve the lowest H-plane X-pol level of no more than −37 dB within the angle range of $|\theta| \le 60^\circ$ while maintaining a reasonable peak gain of 9.8 dBi. For dual linear polarization applications, few existing methods are available. It can be observed in the table that the prototyped dual linearly polarized XSP antenna also achieves the lowest X-pol of lower than −29 dB within about 8.7% fractional bandwidth. It is worth mentioning that the XSP antenna does not occupy additional footprint when compared to its probe-fed patch antenna counterpart, serving a good candidate for an air-filled patch antenna array with a wide scanning angle.

IV. CONCLUSION

A new probe-fed air-filled patch antenna that builds-in the feature of X-pol radiation suppression is proposed and experimentally validated. With legitimate placement of plural floating electrically small metal cylinders, the radiation from the induced currents on the cylinders can theoretically cancel the parasitic H-plane X-pol radiation from the feeding probe. It has been shown that the H-plane X-pol level of a linearly polarized XSP antenna can be reduced to less than −37 dB with respect to the peak co-pol gain for $|\theta| \le 60^\circ$. A 1 × 8 linearly polarized antenna array with the XSP antenna elements is prototyped and measured at different scanning angles, showing a significant improvement on both the co-pol gain and the beam scanning angle range subject to X-pol level when compared to its conventional air-filled patch antenna counterpart. A dual-polarized and wideband version of the XSP antenna is also proposed. The measured maximum X-pol

Authorized licensed use limited to: Chinese University of Hong Kong. Downloaded on July 27,2023 at 06:40:54 UTC from IEEE Xplore. Restrictions apply.

level in all θ-directions can be lower than -29 and -26 dB within an 8.7% fractional bandwidth and the -10 dB reflection coefficient bandwidth, respectively. The new XSP antenna structure does not occupy extra space and the X-pol level can be suppressed in a wide frequency band and wide-angle range without sacrificing other antenna attributes. It is expected that the new probe-fed patch antenna can be a good candidate for phased array antennas where a wide-angle beam scanning is required.

REFERENCES

[1] A. N. Tulintseff, S. M. Ali, and J. A. Kong, "Input impedance of a probe-fed stacked circular microstrip antenna," *IEEE Trans. Antennas Propag.*, vol. 39, no. 3, pp. 381–390, Mar. 1991.

[2] K. M. Luk, C. L. Mak, Y. L. Chow, and K. F. Lee, "Broadband microstrip patch antenna," *Electron. Lett.*, vol. 34, no. 15, pp. 1442–1443, Jul. 1998.

[3] C. L. Mak, K. M. Luk, K. F. Lee, and Y. L. Chow, "Experimental study of a microstrip patch antenna with an L-shaped probe," *IEEE Trans. Antennas Propag.*, vol. 48, no. 5, pp. 777–783, May 2000.

[4] Y. Wang and V. Chandrasekar, "Polarization isolation requirements for linear dual-polarization weather radar in simultaneous transmission mode of operation," *IEEE Trans. Geosci. Remote Sens.*, vol. 44, no. 8, pp. 2019–2028, Aug. 2006.

[5] D. Zrnic, R. Doviak, G. Zhang, and A. Ryzhkov, "Bias in differential reflectivity due to cross coupling through the radiation patterns of polarimetric weather radars," *J. Atmos. Ocean. Technol.*, vol. 27, no. 10, pp. 1624–1637, 2010.

[6] W.-H. Hsu and K.-L. Wong, "Broadband probe-fed patch antenna with a U-shaped ground plane for cross-polarization reduction," *IEEE Trans. Antennas Propag.*, vol. 50, no. 3, pp. 352–355, Mar. 2002.

[7] K.-L. Wong, C.-L. Tang, and J.-Y. Chiou, "Broadband probe-fed patch antenna with a W-shaped ground plane," *IEEE Trans. Antennas Propag.*, vol. 50, no. 6, pp. 827–831, Jun. 2002.

[8] X. Zhang and L. Zhu, "Patch antennas with loading of a pair of shorting pins toward flexible impedance matching and low cross polarization," *IEEE Trans. Antennas Propag.*, vol. 64, no. 4, pp. 1226–1233, Apr. 2016.

[9] N.-W. Liu, L. Zhu, G. Fu, and Y. Liu, "A low profile shorted-patch antenna with enhanced bandwidth and reduced H-plane cross-polarization," *IEEE Trans. Antennas Propag.*, vol. 66, no. 10, pp. 5602–5607, Oct. 2018.

[10] D. Ghosh, S. K. Ghosh, S. Chattopadhyay, S. Nandi, D. Chakraborty, R. Anand, R. Raj, and A. Ghosh, "Physical and quantitative analysis of compact rectangular microstrip antenna with shorted non-radiating edges for reduced cross-polarized radiation using modified cavity model," *IEEE Antennas Propag. Mag.*, vol. 56, no. 4, pp. 61–72, Aug. 2014.

[11] S. Samanta, P. S. Reddy, and K. Mandal, "Cross-polarization suppression in probe-fed circular patch antenna using two circular clusters of shorting pins," *IEEE Trans. Antennas Propag.*, vol. 66, no. 6, pp. 3177–3182, Jun. 2018.

[12] C. Kumar and D. Guha, "Higher mode discrimination in a rectangular patch: New insight leading to improved design with consistently low cross-polar radiations," *IEEE Trans. Antennas Propag.*, vol. 69, no. 2, pp. 708–714, Feb. 2021.

[13] N. W. Liu, L. Zhu, Z. X. Liu, Z. Y. Zhang, G. Fu, and Y. Liu, "Cross-polarization reduction of a shorted patch antenna with broadside radiation using a pair of open-ended stubs," *IEEE Trans. Antennas Propag.*, vol. 68, no. 1, pp. 13–20, Jan. 2020.

[14] H. Chen and K.-L. Wu, "A compact folded air patch antenna with low cross-polarization," in *Proc. 14th Eur. Conf. Antennas Propag. (EuCAP)*, Mar. 2020, pp. 1–3.

[15] A. Petosa, A. Ittipiboon, and N. Gagnon, "Suppression of unwanted probe radiation in wideband probe-fed microstrip patches," *Electron. Lett.*, vol. 35, no. 5, pp. 355–357, Mar. 1999.

[16] C.-Y.-D. Sim, C.-C. Chang, and J.-S. Row, "Dual-feed dual-polarized patch antenna with low cross polarization and high isolation," *IEEE Trans. Antennas Propag.*, vol. 57, no. 10, pp. 3321–3324, Oct. 2009.

[17] Y. P. Zhang and J. J. Wang, "Theory and analysis of differentially-driven microstrip antennas," *IEEE Trans. Antennas Propag.*, vol. 54, no. 4, pp. 1092–1099, Apr. 2006.

[18] Q. Xue, X. Y. Zhang, and C.-H. K. Chin, "A novel differential-fed patch antenne," *IEEE Antennas Wireless Propag. Lett.*, vol. 5, pp. 471–474, 2006.

[19] Z. N. Chen and M. Y. W. Chia, "Broad-band suspended probe-fed plate antenna with low cross-polarization levels," *IEEE Trans. Antennas Propag.*, vol. 51, no. 2, pp. 345–347, Feb. 2003.

[20] P. Li, H. W. Lai, K. M. Luk, and K. L. Lau, "A wideband patch antenna with cross-polarization suppression," *IEEE Antennas Wireless Propag. Lett.*, vol. 3, pp. 211–214, 2004.

[21] H.-W. Lai and K.-M. Luk, "Design and study of wide-band patch antenna fed by meandering probe," *IEEE Trans. Antennas Propag.*, vol. 54, no. 2, pp. 564–571, Feb. 2006.

[22] H.-W. Lai and K.-M. Luk, "Dual polarized patch antenna fed by meandering probes," *IEEE Trans. Antennas Propag.*, vol. 55, no. 9, pp. 2625–2627, Sep. 2007.

[23] C. Sarkar, D. Guha, C. Kumar, and Y. M. M. Antar, "New insight and design strategy to optimize cross-polarized radiations of microstrip patch over full bandwidth by probe current control," *IEEE Trans. Antennas Propag.*, vol. 66, no. 8, pp. 3902–3909, Aug. 2018.

[24] C. Kumar and D. Guha, "Nature of cross-polarized radiations from probe-fed circular microstrip antennas and their suppression using different geometries of defected ground structure (DGS)," *IEEE Trans. Antennas Propag.*, vol. 60, no. 1, pp. 92–101, Jan. 2012.

[25] Y. Luo, Q.-X. Chu, and D.-L. Wen, "A plus/minus 45 degree dual-polarized base-station antenna with enhanced cross-polarization discrimination via addition of four parasitic elements placed in a square contour," *IEEE Trans. Antennas Propag.*, vol. 64, no. 4, pp. 1514–1519, Apr. 2016.

[26] K.-L. Wu, C. Wei, X. Mei, and Z.-Y. Zhang, "Array-antenna decoupling surface," *IEEE Trans. Antennas Propag.*, vol. 65, no. 12, pp. 6728–6738, Dec. 2017.

Hao Chen received the B.S. degree from the University of Electronic Science and Technology of China, Chengdu, China, in 2014. He is currently pursuing the Ph.D. degree with The Chinese University of Hong Kong, Hong Kong.

From 2014 to 2016, he was an Antenna Engineer with Shenzhen Sunway Communication Company Ltd., Shenzhen, China. He holds 16 granted patents. His current research interests include antenna designs for wireless applications and self-decoupled MIMO antennas for mobile terminals.

Ke-Li Wu (Fellow, IEEE) received the B.S. and M.Eng. degrees from the Nanjing University of Science and Technology, Nanjing, China, in 1982 and 1985, respectively, and the Ph.D. degree from Laval University, Quebec, QC, Canada, in 1989.

From 1989 to 1993, he was a Research Engineer with McMaster University, Hamilton, ON, Canada. He joined COM DEV (now Honeywell Aerospace), Cambridge, ON, Canada, in 1993, where he was a Principal Member of Technical Staff. Since 1999, he has been with The Chinese University of Hong Kong, Hong Kong, where he is currently a Professor and the Director of the Radio Frequency Radiation Research Laboratory. His current research interests include EM-based circuit domain modeling of high-speed interconnections and radiation problems, robot automatic tuning of microwave filters, decoupling techniques of multi-input and multi-output (MIMO) antennas, and Internet of Things (IoT) technologies.

Dr. Wu is a member of the IEEE MTT-5 Filters Committee of Microwave Theory and Techniques Society. He was a recipient of the 1998 COM DEV International Ltd., Achievement Award and the Asia–Pacific Microwave Conference Prize twice in 2008 and 2012, respectively. He was an Associate Editor of the IEEE TRANSACTIONS ON MICROWAVE THEORY AND TECHNIQUES from 2006 to 2009.

Authorized licensed use limited to: Chinese University of Hong Kong. Downloaded on July 27,2023 at 06:40:54 UTC from IEEE Xplore. Restrictions apply.